THE JOURNAL OF PHYSICAL CHEMISTRY Letters

Perspective

pubs.acs.org/JPCL

Nanotubes from Misfit Layered Compounds: A New Family of Materials with Low Dimensionality

Leela S. Panchakarla,[†,∥] Gal Radovsky,[†,∥] Lothar Houben,[‡] Ronit Popovitz-Biro,[§] Rafal E. Dunin-Borkowski,[‡] and Reshef Tenne*[,†]

[†]Department of Materials and Interfaces and [§]Chemical Research Support Department, Weizmann Institute of Science, Rehovot, 76100 Israel

[‡]Ernst Ruska-Centre for Microscopy and Spectroscopy with Electrons and Peter Grünberg Institute, Forschungszentrum Jülich, D-52425 Jülich, Germany

ABSTRACT: Nanotubes that are formed from layered materials have emerged to be exciting one-dimensional materials in the last two decades due to their remarkable structures and properties. Misfit layered compounds (MLC) can be produced from alternating assemblies of two different molecular slabs with different periodicities with the general formula $[(MX)_{1+x}]_m[TX_2]_n$ (or more simply MS-TS_2), where M is Sn, Pb, Bi, Sb, rare earths, T is Sn, Nb, Ta, Ti, V, Cr, and so on, and X is S, Se. The presence of misfit stresses between adjacent layers in MLC provides a driving force for curling of the layers that acts in addition to the elimination of dangling bonds. The combination of these two independent forces leads to the synthesis of misfit layered nanotubes, which are newcomers to the broad field of one-dimensional nanostructures and nanotubes. The synthesis, characterization, and microscopic details of misfit layered nanotubes are discussed, and directions for future research are presented.

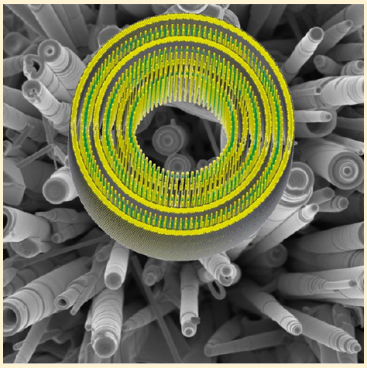

Surfaces are, in general, considered to be different from the corresponding bulk materials. This difference is especially pronounced in nanomaterials, in which the majority of the atoms can reside at the surface. Hollow-closed nanostructures that are formed from low-dimensional materials, such as layered two-dimensional (2D) compounds, exhibit fewer pronounced differences between the surface and the bulk. As a result, nanotubes that are made from inorganic layered materials provide unique opportunities to study properties that are only weakly affected by unsaturated surface bonding and defects. A large number of layered materials can be folded into nanotubes, including carbon, WS_2, MoS_2, BN, and SnS_2.[1−4] Some of these materials, such as WS_2 and BN, can be manufactured in kg/batch quantities. "Industrial grade" fullerene-like nanostructures of WS_2, were commercialized as superior lubricants, and are produced in mass quantities.

"Industrial grade" fullerene-like nanostructures of WS_2, were commercialized as superior lubricants, and are produced in mass quantities.

Incommensurate composite crystals are formed from alternating stackings of two independent constituents that have different lattice periodicities. Examples of these classes of materials are metal-chalcogenide misfit layer compounds (MLC) that have the general formula $[(MX)_{1+x}]_m[TX_2]_n$ where M is Sn, Pb, Bi, Sb, rare earths, T is Sn, Nb, Ta, Ti, V, Cr, and so on, and X is S, Se.[5−7] The alternating layers in each MX and TX_2 subsystem (in short O−T, where O and T stand for MX and TX_2 subunits, respectively) have different crystal structures. MX can be regarded as a molecular slice (layer) cut from the (001) plane of a distorted NaCl structure, while the three-atom thick TX_2 molecular layer can be regarded as a slice cut from a lattice with a pseudohexagonal structure. The interaction between these subsystems manifests itself as a mutual incommensurate structural modulation, i.e., their structures are distorted from those of the bulk phases.[5] Compounds that do not have three-dimensional (3D) structures in bulk form, such as CrS_2, often adopt layered structures when forming part of an MLC lattice. Furthermore, MX compounds with stoichiometries that do not exist as bulk phases, such as SbS, may be stable as part of MS-TS_2 MLC. After the formation of a mutual structural modulation, the in-plane periodicities of the different layer types are usually incommensurate along at least one direction.[5−7] It is then not possible to define a common unit cell, and the final superstructure lacks 3D periodicity. Therefore, a precise description of the atomic positions in an entire $[(MX)_{1+x}]_m[TX_2]_n$ system requires the use of one or two modulation vectors in addition to three conventional vectors in 3D space.[5] The number of required additional vectors depends on the nature of the interaction and on the mutual structural modulation of the two subsystems. In general, layered materials

Received: August 10, 2014
Accepted: October 9, 2014

   dx.doi.org/10.1021/jz5016845 | J. Phys. Chem. Lett. 2014, 5, 3724−3736

have strong intralayer bonding, with the layers stacked together via weak van-der-Waals and polar forces. MLC show stronger interlayer bonding, in addition to van-der-Waals forces, as a result of partial charge transfer. The structures of MLC can be associated closely with those of the well-known 2D-natured high T_c cuprates, or more generally with ternary metal-oxide perovskites. However, in contrast to oxides that are highly ionic in nature, chalcogenide-based mistfit compounds possess strongly covalent bonds between the atoms within each layer. Misfit compounds often have superior properties when compared with those of the individual constituents. For instance, 2H-TaS_2 becomes superconducting at a critical temperature (T_c) of 0.65 K, whereas the PbS intercalated misfit compound of TaS_2, i.e., PbS−TaS_2, has a T_c of 3.1 K.[5] Several reviews are devoted to the structures and physical properties of these materials in bulk form.[5,7] The present "Perspective" focuses on nanotubular structures that are generated from these fascinating compounds. Due to their layered structures, nanotubes of misfit layered compounds can be synthesized and the properties offered by their unique structure, chemistry and reduced dimension can be exploited. Recent advances in synthesis and characterization, as well as selected physical properties conferred to the misfit nanotubes by their reduced dimension, are described. Potential properties that may be realized in the near future by studying these materials are discussed.

Due to their layered structures, nanotubes of misfit layered compounds can be synthesized and the properties offered by their unique structure, chemistry and reduced dimension can be exploited.

Synthesis and Mechanism of Formation. One of the main driving forces for the formation of hollow-closed cages and in particular rolled structures of layered (2D) compounds at the nanoscale is the minimization of the high energy of the unsaturated rim atoms.[3,8] MLC, in particular, also fold into rolled structures as a result of misfit strain between the two constituent subunits,[9,10] making them ideal candidates to form nanotubular structures. Bernaerts et al. first observed micron-sized cylindrical and conical scrolls of metal chalcogenide MLC in the $(PbS)_{1+x}(NbS_2)_n$[9] and $(BiS)_{1+x}(NbS_2)_n$ systems.[11] However, nanostructures of these compounds (and MLC in general) were not explored until recently. SnS−SnS_2 is, in fact, the first misfit compound to be synthesized in nanotubular form.[10] Laser ablation of a SnS_2 target with a Nd:YAG laser was used to form short tubular nanostructures comprising SnS and SnS_2 molecular layers.[10] One of the slabs was shown to consist of a two-atom-thick double layer of atoms, each with an equal number of Sn and S atoms (SnS), while the other slab consisted of a three-atom-thick sandwich of a Sn layer between two layers of S atoms (SnS_2). Two types of MS-TS_2 (in short O-T) superstructures: (a) O−O−T−O−O−T... and (b) O−T−O−T... could be resolved in the product. Presumably, excessive evaporation of S from the SnS_2 target upon laser irradiation resulted in S-deficiency, promoting the spontaneous formation of the misfit superstructures.

Chemical and physical vapor transport (CVT/PVT) has been used in the synthesis of a wide variety of nanotubes from MLC. Here, powders of the precursors are inserted into a quartz ampule. Although powders of the elemental metals are used in many cases, sulfides can also be used, as detailed in Table 1. Excluding the case of SnS−SnS_2, chlorine is used as a transport agent. Sources of chlorine are typically chlorides of the metals constituting the MLC. In general, high temperature annealing involves two steps, in which the ampule is placed in different quite steep temperature gradients, as detailed in previous publications.[12−15] An example of a partially rolled SbS−TaS_2 MLC sheet produced by the CVT technique is shown in Figure 1.

The primary driving force for the formation of tubular structures from MLC is the misfit between the MX and the TX_2 layers. Upon scrolling, the strain energy associated with the misfit is reduced. In addition, as a result of the presence of atoms with dangling bonds on their rims, nanoparticles of compounds with layered structures are unstable in planar form and fold into seamless hollow structures, such as nanotubes. It is shown here that the combination of these two stimuli leads to the formation of new kinds of nanotubes from MLC. The presence of dislocation-like defects on their surfaces suggests that the transition from scroll-like to concentric tubules is likely to occur by a mechanism that involves high-temperature dislocation motion.

Nanotubular structures have been synthesized for a large number of MLC, as listed in Table 1. The precursors and growth techniques for these compounds are also summarized in this table. For most of the compounds, the lattice parameters of the MS and TS_2 subsystems have been determined. The TX_2 layer is defined by an ortho-pseudohexagonal (a, $\sqrt{3}\cdot a$) unit cell. Therefore, the lattice parameters of orthorhombic MS−TS_2 MLC with (T = Nb, Ta; M = Pb, Sn, most of the rare earth elements) are described accurately. Here T atoms are in trigonal prismatic coordination with respect to S atoms. In MLC with (T = V, Cr), the T atoms are in octahedral (trigonal antiprismatic) coordination with respect to the S atoms. Small monoclinic/triclinic distortions that may occur in MLC nanotubes have not been deduced from selected area electron diffraction (SAED) patterns with confidence.

Tubular structures synthesized from SnS−SnS_2,[12,13] PbS−NbS_2,[14] and MS−TaS_2 (with M = Pb, Sn, Sb, Bi) MLC compounds[15] were synthesized by the physical/chemical transport method in evacuated silica tubes. The synthesis included two main steps, with the silica tubes placed in appropriate temperature gradients.[12−15] In all cases, the products were collected from the cold zone of the tube, and their structures were studied in detail.[13−15] Very recently, tubular structures of $(LaS)_{1.13}TaS_2$ MLC were also synthesized in evacuated silica tubes. However, they were found to be produced in the hot zone of the silica tube. The details of the synthesis and analysis of their structures will be published elsewhere.

Structural Properties. Figure 2a−c shows an agglomerate of SbS−TaS_2 MLC tubular crystals with a large variety of outer diameters, varying between 60 nm and 5 μm. The ratios between the inner and outer diameters can be close to the limiting values of 0 and 1. Figure 2d−f shows an agglomerate of LaS-TaS_2 MLC tubular crystals. These tubules exhibit greater uniformity of their diameters, with typical outer diameters in the range 200−500 nm. The ratios between the inner and outer diameters are typically below 0.5. Scrolling steps are encountered in both the SbS−TaS_2 and the LaS−TaS_2 cases. However, they are more pronounced for SbS−TaS_2.

Details of the structures of PbS−NbS_2 tubular crystals, which are given below, highlight the complexity of the structures of

dx.doi.org/10.1021/jz5016845 | J. Phys. Chem. Lett. 2014, 5, 3724−3736

Table 1. Summary of Data for Misfit Nanotubes: Synthesis Procedure and Lattice Parameters Obtained from Electron Diffraction

				lattice parameters (Å)		
compound	precursors	growth technique		*a*	*b*	*c*
LaS−CrS_2	mixture of $La(OH)_3$ and $Cr(OH)_3$ or $LaCrO_3$ powder	thermal annealing[c]	LaS	6.02 (5.752)	6.02 (5.936)	11.3[16] (11.04)[5]
			CrS_2	3.44 (3.435)	6.02 (5.936)	11.3[16] (11.05)[5]
CeS−CrS_2	mixture of $Ce(OH)_3$ and $Cr(OH)_3$	thermal annealing[c]	CeS	6.0	6.0	11.2[16]
			CrS_2	3.44	6.0	11.2[16]
GdS−CrS_2	mixture of $Gd(OH)_3$ and $Cr(OH)_3$	thermal annealing[c]	GdS	5.82 (5.454)	6.26 (5.810)	11.0[16] (21.46)[5]
			CrS_2	3.7 (3.451)	6.26 (5.802)	11.0[16] (21.46)[5]
TbS−CrS_2	mixture of $Tb(OH)_3$ and $Cr(OH)_3$	thermal annealing[c]	TbS	5.66	5.28	10.5[16]
			CrS_2	3.34	5.28	10.5[16]
YS−CrS_2	mixture of $Y(OH)_3$ and $Cr(OH)_3$	thermal annealing[c]	YS	5.34 (5.41)	5.82 (5.78)	10.7[16] (10.7)[5]
			CrS_2	3.39 (3.46)	5.82 (5.78)	10.7[16] (10.7)[5]
LaS−VS_2	mixture of $La(OH)_3$ and $VOSO_4$	thermal annealing[c]	LaS	6.02 (5.705)	6.02 (5.828)	11.4[16] (22.32)[17]
			VS_2	3.44 (3.366)	6.02 (5.828)	11.4[16] (22.32)[17]
$La_{1-x}Sr_xS$−CrS_2	mixture of $La(OH)_3$, $Sr(OH)_2$ and $Cr(OH)_3$	thermal annealing[c]	$La_{1-x}Sr_xS$	5.82	5.82	11.1[16]
			CrS_2	3.44	5.82	11.1[16]
$La_{1-x}Ce_xS$−CrS_2	mixture of $La(OH)_3$, $Ce(OH)_3$ and $Cr(OH)_3$	thermal annealing[c]	$La_{1-x}Ce_xS$	6.0	6.0	11.3[16]
			CrS_2	3.5	6.0	11.3[16]
$La_{1-x}Gd_xS$−CrS_2	mixture of $La(OH)_3$, $Gd(OH)_3$ and $Cr(OH)_3$	thermal annealing[c]	$La_{1-x}Gd_xS$	5.94	5.94	11.2[16]
			CrS_2	3.48	5.94	11.2[16]
$La_{1-x}Eu_xS$−CrS_2	mixture of $La(OH)_3$, $Eu(OH)_3$ and $Cr(OH)_3$	thermal annealing[c]	$La_{1-x}Eu_xS$	5.86	5.86	11.3[16]
			CrS_2	3.42	5.86	11.3[16]
$Ce_{1-x}Gd_xS$-Crs_2	mixture of $Ce(OH)_3$, $Gd(OH)_3$ and $Cr(OH)_3$	thermal annealing[c]	$Ce_{1-x}Gd_xS$	5.93	5.93	11.2[16]
			CrS_2	3.47	5.93	11.2[16]
PbS−NbS_2	mixture of Nb, PbS, S, and $PbCl_2$/$NbCl_5$	CVT	PbS	5.78 (5.834)	5.76 (5.801)	11.9[14] (11.9)[5]
			NbS_2	3.34 (3.313)	5.76 (5.801)	11.9[14] (23.8)[5]
PbS−TaS_2	mixture of Ta, PbS, S, and $TaCl_5$	CVT	PbS	5.66 (5.825)	5.74 (5.779)	12.3[15] (23.96)[5]
			TaS_2	3.3 (3.304)	5.74 (5.779)	12.3[15] (23.96)[5]
SnS−TaS_2	mixture of Ta, SnS_2, S, and $TaCl_5$	CVT	SnS	5.72 (5.737)	5.74 (5.749)	12.4[15] (11.88)[5]
			TaS_2	3.32 (3.308)	5.74 (5.75)	12.4[15] (23.76)[5]
BiS−TaS_2	mixture of Ta, Bi, S, and $TaCl_5$	CVT	BiS	(6.101)	(5.725)	11.7[15] (23.07)[5]
			TaS_2	(3.3)	(5.732)	11.7[15] (23.14)[5]
SbS−TaS_2	mixture of Ta, Sb, S, and $TaCl_5$	CVT	SbS			11.7[15] (11.51)[5]
			TaS_2			11.7[15] (11.51)[5]
LaS−TaS_2	mixture of Ta, La, S, and $TaCl_5$	thermal annealing	LaS	5.72 (5.813)	5.62 (5.775)	11.3[cur] (11.53)[5]
			TaS_2	3.26 (3.295)	5.62 (5.775)	11.3[cur] (23.06)[5]
SnS−SnS_2	mixture of SnS_2, SnS, Bi, and Sb_2S_3.	PVT	SnS	4.32[a] (4.32)	3.96[a] (3.98)[18]	11.5[13]
			SnS_2	3.64[b] (3.648)	3.64[b] (3.648)[19]	11.5[13]

Lattice parameters were calculated from data published in the specified references ("cur" means current work where the details will be published elsewhere). The lattice parameters of TS_2 are given according to the ortho-pseudohexagonal (a, $\sqrt{3}\cdot a$) unit cell of TS_2. This system is an approximation for the octahedral CrS_2 and the VS_2 based MLC, in which the angles of the unit cells deviate by up to several degrees from 90°. The values in brackets are included for comparison and were deduced mostly from the XRD analysis of single crystal/micro crystallite (planar) powder samples or ED patterns of thin platelets along the [001] zone axis. [a]In-plane lattice parameters according to the definitions of Herzenbergite.[18] [b]In-plane lattice parameters according to the pseudohexagonal unit cell. [c]Thermal annealing is performed in the presence of H_2 and H_2S.

MLC tubular crystals. Tubes of PbS−NbS_2 MLC are isostructural with PbS−TaS_2 and have much in common with their SnS−TaS_2 counterparts.[14,15] In MLC $(MS)_{1+y}(TS_2)$ where (M = Pb, Sn, most of the rare earths; T = Nb, Ta), Nb or Ta atoms in the NbS_2 (TaS_2) subsystems are in trigonal prismatic coordination with S, which results in orthorhombic unit cells for both the TX_2 and the MX subsystems.[5,7] Exceptions are seen for $(SbS)_{1.14}NbS_2$ and $(SbS)_{1.16}TaS_2$ MLC,[20] in which both subsystems exhibit triclinic distortions due to a complex interaction. SbS, which is not known as a bulk phase, becomes stable as monolayers within the MLC, exhibiting a complex structure.[15,21,22]

Figure 3a shows the results of a TEM study of a PbS-NbS_2 MLC tubule, in which PbS and NbS_2 layers are stacked periodically along the common *c*-axis. Much of the structural information can be deduced from the analysis of the SAED pattern of the tubule. The 1.19 nm periodicity of the structure can be verified from the line profile and the basal reflections in the SAED pattern (marked by blue arrows). Spots corresponding to the same interplanar spacings are marked by segmented circles, alongside the respective Miller indices. Spots originating from the TX_2 layers (NbS_2 in this case) are marked in red, using the pseudohexagonal system for indexing. However, it is also convenient to index the TX_2 layer in the ortho-pseudohexagonal system with in-plane lattice parameters of a and $b = \sqrt{3}\cdot a$, as shown in the model in Figure 4 (layer 1 of NbS_2), where a is the lattice parameter of the pseudohexagonal unit cell.[14] Spots with interplanar spacings of 2.88 and 1.67 Å are attributed to the (10.0) and (11.0) planes of NbS_2, respectively, in the pseudohexagonal system (equivalent to the (020) and (200) planes in the ortho-pseudohexagonal system). The multiplicity factor, i.e., the number of equivalent planes, is 6. However, the

dx.doi.org/10.1021/jz5016845 | J. Phys. Chem. Lett. 2014, 5, 3724−3736

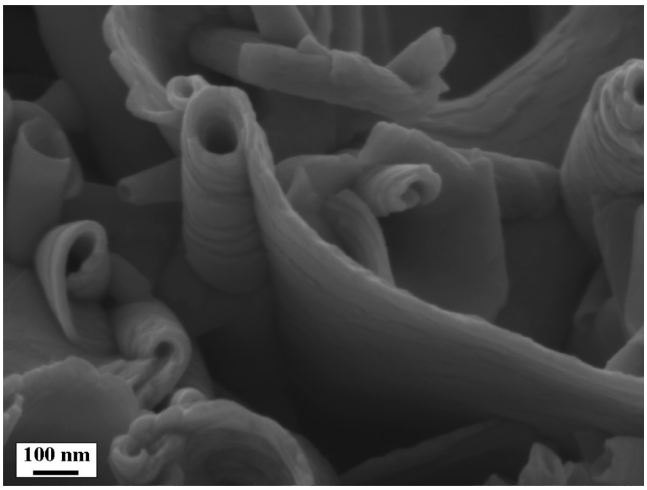

Figure 1. Scanning electron microscope (SEM) image of partially rolled SbS−TaS_2 sheets.

diffraction pattern shows 12 pairs of spots that are distributed equal-azimuthally in a ring-like pattern, with an azimuthal angle between any two adjacent pairs of spots of 30°. This observation suggests that there are two groups of NbS_2 layers with different folding vectors within the tubule. These two groups of NbS_2 layers produce two sextets of interlocked spots, which are encircled by red and orange small circles of (10.0) and (11.0) reflections. The azimuthal angle between the two sextets of spots equals the azimuthal angle between two adjacent sets of (11.0) or (10.0) spots, which is 30°, as marked in the SAED pattern-repetition. It is apparent that both the (10.0) and the (11.0) spots of NbS_2 coincide with the tube axis (marked by a long purple double arrow). However, the coincident (10.0) and (11.0) spots originate from different NbS_2 layers with different folding vectors in the MLC nanotube. When the (10.0) reflection coincides with the tubule axis, the layer is termed "zigzag-like", while when the (11.0) reflection coincides with the tubule axis it is termed "armchair-like". Therefore, two groups of NbS_2 layers exist in this tube with different folding vectors. The "zigzag-like" (10.0) folding spots are marked by small red circles, while the "armchair-like" (11.0) spots are marked by small orange circles. The two groups of NbS_2 layers are shown in the schematic model in Figure 4 and are denoted by red "1" and orange "2" symbols. These colors correspond to the colors of the small circles that mark the respective spots in Figure 3a.

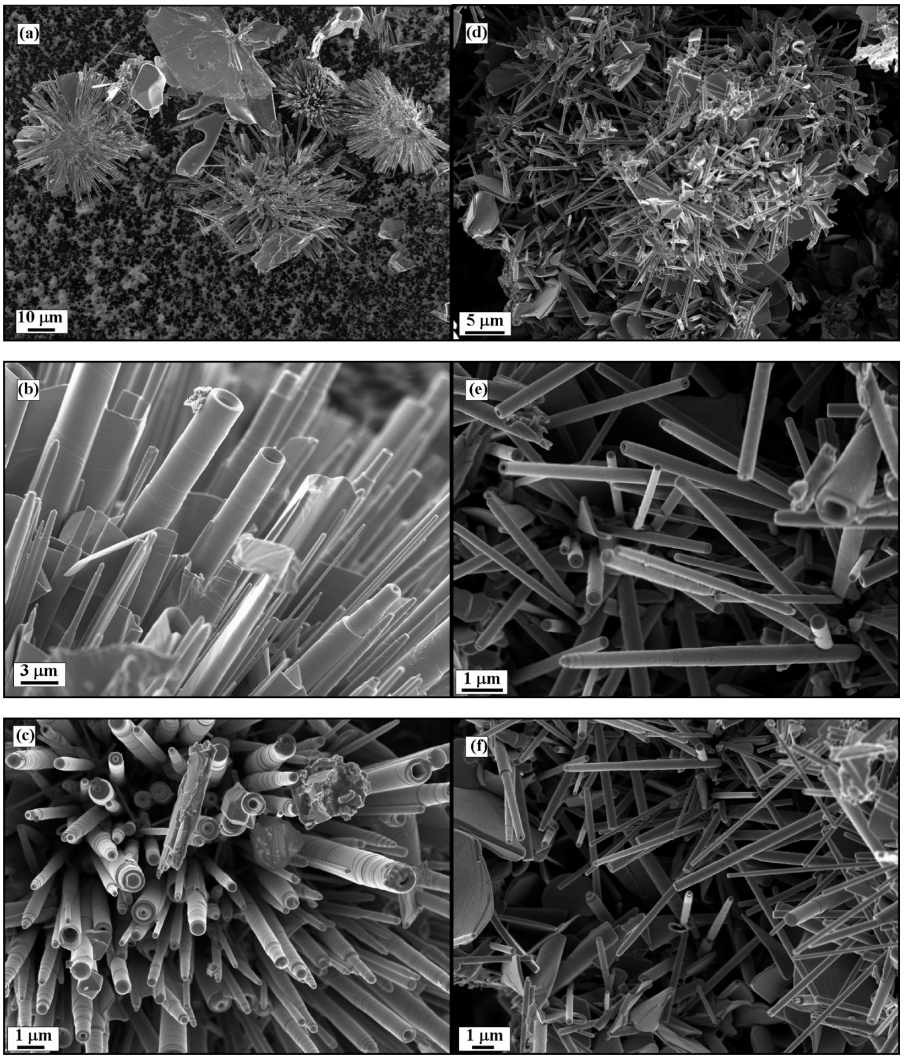

Figure 2. SEM images of (a−c) SbS−TaS_2 and (d−f) LaS−TaS_2 tubular crystals.

dx.doi.org/10.1021/jz5016845 | *J. Phys. Chem. Lett.* 2014, 5, 3724−3736

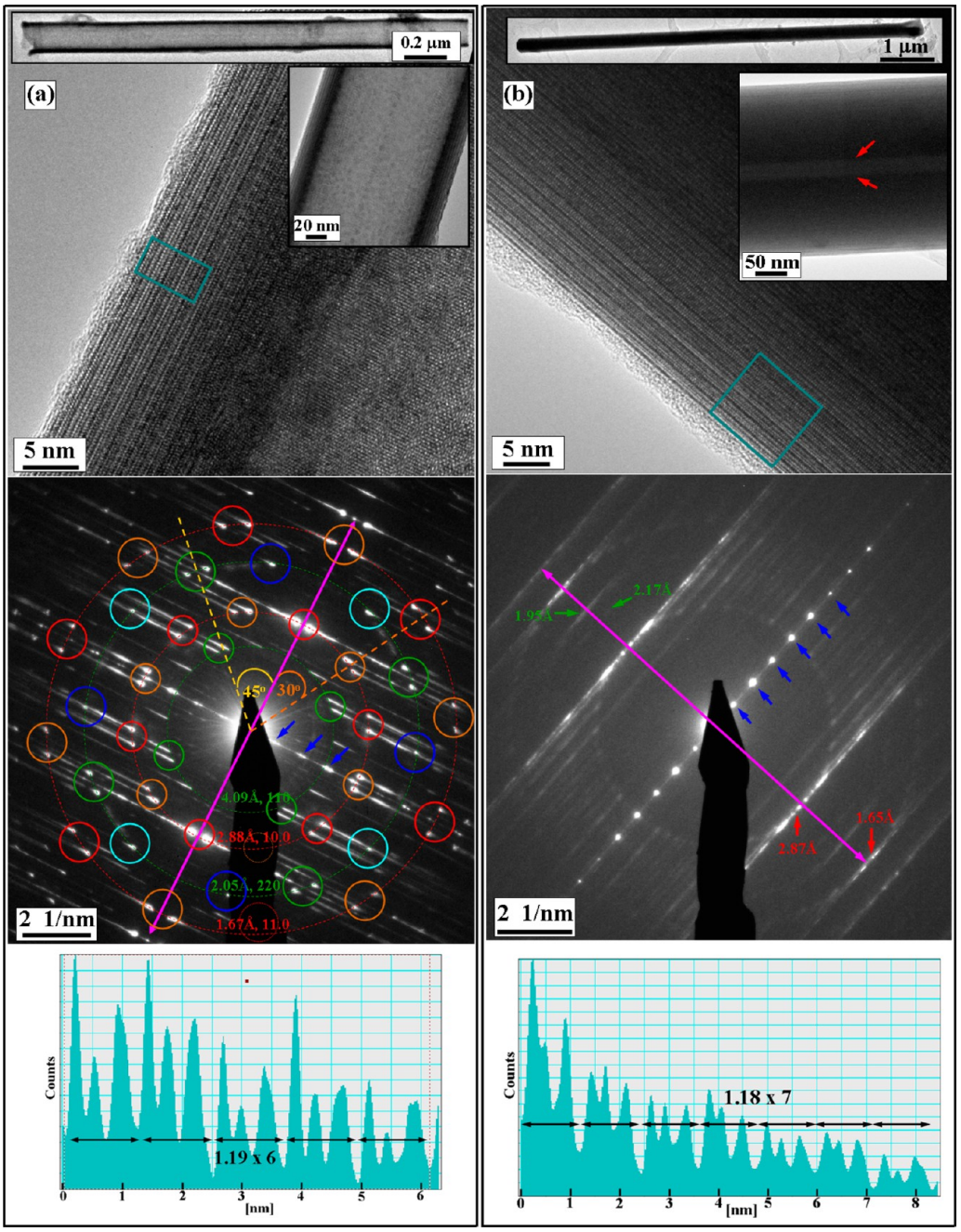

Figure 3. (a) TEM images of a PbS-NbS_2 nanotube with PbS and NbS_2 layers stacked periodically along the *c*-axis with 1.19 nm periodicity. Top: High, medium and low magnification images. Middle: selected area electron diffraction pattern acquired from the area shown in the high magnification image. Spots corresponding to the same interplanar spacing are marked by segmented circles and their corresponding Miller indices are noted. (Red circles correspond to NbS_2 and green to PbS). The tubule axis is marked by a purple double arrow. The small blue arrows indicate basal reflections produced by the superstructure. See text for an explanation of the small circles. Bottom: Line profile of the contrast obtained from the region enclosed in the rectangle in the high magnification image. (b) TEM images of a SbS-TaS_2 tubule with SbS and TaS_2 layers stacked periodically along the *c*-axis with 1.18 nm periodicity. Top: High magnification image, with medium and low magnification images in the insets. The narrow hollow core is marked by small red arrows. Middle: SAED pattern acquired from the area shown in the high magnification image. Spots corresponding to the same interplanar spacing are distributed in ring-like patterns. Their measured interplanar spacings are indicated (red: TaS_2, green: SbS). The tubule axis is marked by a purple double arrow. The small blue arrows indicate basal reflections produced by the superstructure. Bottom: Line profile of the contrast obtained from the region enclosed in the rectangle in the high magnification image.

As a result of the chirality of the NbS_2 shells, all of the (10.0) and (11.0) pairs of spots are splintered by an azimuthal angle of 7.5° in this case. This splitting reflects the small difference in atomic lattice orientation within the layers between the top and bottom parts of the tubule. The chiral angle is half of the azimuthal angle, which is $7.5/2 \approx 3.8°$ in this case.

Spots with interplanar spacings of 4.09 and 2.05 Å are attributed to the (110) planes and the second-order (220) planes of PbS, respectively. Here, 12 sets of spots, which are equally azimuthally distributed on a circle, are observed. However, the multiplicity factor of these planes is 4 (orthorhombic symmetry). Consequently, three groups of PbS layers with different folding

dx.doi.org/10.1021/jz5016845 | *J. Phys. Chem. Lett.* 2014, 5, 3724−3736

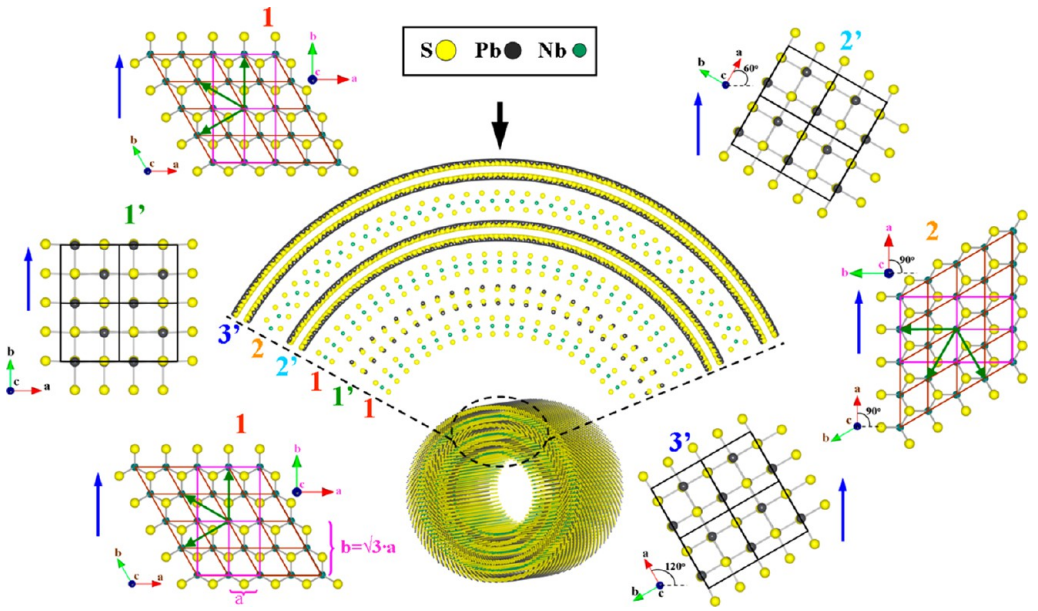

Figure 4. Schematic model showing the stacking of the PbS and the NbS_2 layers along their common *c*-axis and their in-plane orientations for the tubule shown in Figure 3a. Two types of NbS_2 layers are denoted "1" and "2", respectively. Three types of PbS layers are denoted "1′", "2′" and "3′", respectively. The colors of the symbols correspond to the colors of the small circles that mark the corresponding spots. For every layer, a head-on view along the *c*-axis is shown (assuming a flat layer in the area marked by the black arrow) and the tubule axis is marked by blue arrows. For the NbS_2 layers, pseudohexagonal and ortho-pseudohexagonal unit cells are shown using brown and purple cells, respectively. The relationship between the two is shown in the bottom left NbS_2 type "1" head-on view. Three equivalent "*b*" directions are indicated by green arrows, according to the ortho-pseudohexagonal unit system, in all NbS_2 projections.

vectors occur in this tubule. Three quartets of (220) spots are marked by small green, cyan, and blue circles (only one quartet of (110) spots is marked by green small circles for convenience). These three quartets are rotated azimuthally by 60° and 120° relative to each other about the common *c*-axis. Analogously to the situation for the NbS_2 layers, three groups of PbS layers exist in this tube. They are shown in the schematic model in Figure 4 and marked with green "1′", cyan "2′" and blue "3′" symbols. Group 2′ PbS layers (cyan circles) and group 3′ PbS layers (blue circles) are rotated by 60° and 120° with respect to group 1 PbS layers (small green circles) about the common *c*-axis. Interestingly, spot splitting, which results from the chiral nature of the layers, only occurs for group 1′ PbS layers in this tubule. The chiral angle of this group (green circles) is ∼3.8°. The other two quartets of spots, which are marked by small cyan and blue circles, do not appear to exhibit chiral splitting. This situation is only rarely encountered. In the vast majority of cases, all of the PbS layers within a tubule exhibit similar chiral angles.[14,15]

The folding vectors and relative orientations of the PbS and NbS_2 layers can be determined from the azimuthal positions of their spots. A model of the entire tubule is shown in Figure 4. In the tube shown in Figure 3a, one quartet of (110) spots and their second-order (220) spots, which are marked by small green circles, form an angle of ∼45° with respect to the tubule axis, as shown in the diffraction pattern. The angle between the (110) and (010) planes of the PbS layer in bulk $(PbS)_{1.14}NbS_2$ MLC is 44.84° (∼45°). Therefore, for the group of PbS layers represented by this quartet of spots (green circles), the normal to the (010) planes (the *b*-axis) coincides with the tubule axis. However, the (010) reflections of PbS do not appear in the SAED pattern, and their second-order (020) reflections coincide with that of (10.0) of NbS_2 (or (020) in the ortho-pseudohexagonal system). This situation occurs because in bulk PbS-NbS_2 MLC the *b*-axis is commensurate and common to both the PbS and the NbS_2 system. In the present nanotube, the normal to the (020) planes of PbS belonging to group 1′ is parallel to the normal to the group 1 (10.0) planes of NbS_2 and both coincide with the tubule axis. Two additional groups of PbS layer quartets of spots, which are represented by cyan (group 2′) and blue (group 3′) circles, form equivalent orientations relative to the NbS_2 layer (of group 1) due to the 6-fold symmetry. However, their orientations relative to the tubule axis are different to that of PbS layers belonging to group 1′ (green circles).

NbS_2 walls belonging to group 2 in Figure 3a (marked by small orange circles) are rotated by 30° with respect to the planes belonging to group 1 (small red circles), as stems from the two sextets of spots. However, a rotation by 30° is equivalent to 90° (30 + 60 = 90°) due to the 6-fold symmetry of the NbS_2 layers. Therefore, the group 2 layers of NbS_2 in Figure 3a (and in the model shown in Figure 4) have different in-plane orientations relative to all three groups of the PbS layers. Here, the normal to the (10.0) planes (the 020 planes in ortho-pseudohexagonal indexing − the *b*-axis) of NbS_2 are parallel to the normal to the (100) planes of PbS − the *a*-axis, instead of the normal to the (010) plane. The angle between the (200) and (020) planes in PbS is 90°, which is similar to the rotation of the NbS_2 layers belonging to group 1 (red circles) relative to group 2 (orange circles). Since the *a* and *b* axes of PbS in the PbS-NbS_2 MLC are almost equal (5.801/5.834) = 0.994 ≈ 1,[5] the energy associated with the small misfit between the *b*-axis of NbS_2 and the *a*-axis of PbS is rather small. Therefore, instead of the two *b* parameters of the two subsystems coinciding, here the *b* parameter of NbS_2 coincides with the *a* parameter of PbS.

The structure of SbS-TaS_2 nanotubes is different from that of PbS-NbS_2. An example of such a tubule is shown in Figure 3b. Here, the TaS_2 and SbS layers are stacked periodically along the *c*-axis with 1.18 nm periodicity, as shown in the line profile and

dx.doi.org/10.1021/jz5016845 | J. Phys. Chem. Lett. 2014, 5, 3724−3736

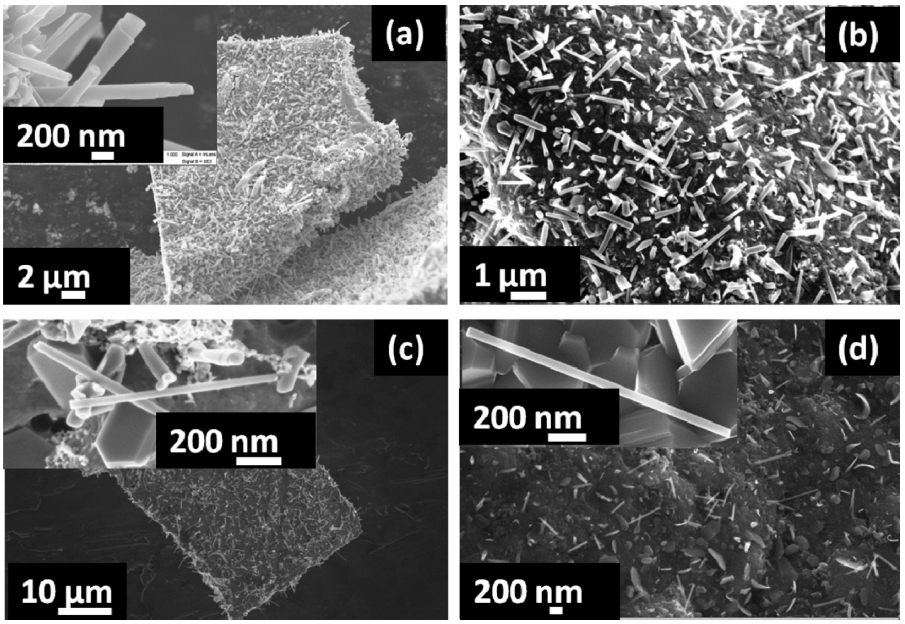

Figure 5. SEM images of (a) LaS-CrS_2 (b) CeS-CrS_2, (c) GdS-CrS_2 and (d) TbS-CrS_2 nanoscrolls and nanotubes. Insets show corresponding high-resolution SEM images.

confirmed by the distance between the basal reflections in the SAED pattern. In contrast to PbS, SnS and many rare earth sulfides, SbS does not exist as a bulk phase. It is stabilized as monolayers between the TX_2 layers in the MLC. In the well-known Sb_2S_3 (stibnite) compound, the valency of Sb is +3. Highly complex models describing the structure of SbS in the corresponding MLC were proposed based on XRD analysis,[21] which was also supported by photoelectron spectroscopy measurements.[23] It was proposed that the monolayers of SbS consist of two phases: one a normal rock-salt-like structure and the second comprising zigzag chains of Sb−Sb and S−S bonds that build up at the antiphase boundaries.[21,23] Sb atoms were found to exist in an oxidation state of +3, as well as in metallic form, in this case.

In the SAED patterns of a vast majority of SbS-TaS_2 tubes, almost ring-like patterns of spots were observed.[15] Due to the large thickness of the tube shown in Figure 3b, these rings are weak, although they are still observable. Examples of thinner tubes with more intense rings of spots are shown elsewhere.[15] Interplanar spacings corresponding to the ring-like patterns of spots are indicated on the pattern. However, due to the triclinic distortion of both the SbS and the TaS_2 layers in this MLC,[20] Miller indexing of the planes is rather difficult. Spots with interplanar spacings of 1.65 and 2.87 Å are close to those of the (11.0) and (10.0) planes of 2H-TaS_2.[24] Rings with interplanar spacings of 2.15 and 2.17 Å are attributed to SbS. The ring-like patterns of spots suggest a turbostratic disorder (misorientation) of the layers about the common *c*-axis. Therefore, the relative in-plane (*a*-*b*) orientations of the SbS and TaS_2 layers cannot be determined easily. However, the very existence of such stable MLC nanotubes, consisting of a lattice with alternating SbS and TaS_2 molecular layers, suggests that their relative orientation is not random. Nevertheless, multiple stacking orders of the molecular sheets are possible. Therefore, it is believed that these ring-like patterns arise from turbostratic misorientation between the SbS-TaS_2 slabs.

Combinations of rare earth and 3d transition metals are known to form MLC with unique properties.[5,6,25] Misfit compounds with the formula LnS-TS_2 (Ln=lanthanide and T=3d element) have interesting two-dimensional magnetic properties, where both the M=Ln and T metal ions are magnetic.[5] The magnetic properties can be tuned by selecting the Ln or T elements, for example Gd and Cr atoms, respectively.[25] Furthermore, by choosing an appropriate combination of elements, one can tailor the electronic characteristics of the MLC to form an insulator, a semiconductor, a metal or a low temperature superconductor. Light-emitting properties can also be obtained from compounds containing some of the lanthanide elements.

Chemical vapor transport of lanthanide sulfides with 3d transition metal sulfides was found to be unsuccessful. Recently, a simple method was developed to synthesize nanotubular structures from a wide variety of lanthanide-based 3d transition metal misfit sulfides by high temperature thermal annealing of the respective ternary oxides or hydroxide mixtures in the presence of H_2 and H_2S.[16] A representative SEM image of as-prepared LaS-CrS_2 nanotubes synthesized at 900 °C is shown in Figure 5a. Vertical growth of nanotubes and nanoscrolls springing out from the originally ternary oxide substrate can be seen. The average diameter of the nanotubular structures is 150 nm, while their lengths range from 500 nm to 3 μm. The size and yield of the nanotubes can be tuned by the reaction conditions. Several nanotubular structures were prepared by this method (see Table 1). SEM images of CeS-CrS_2, GdS-CrS_2 and TbS-CrS_2 nanotubular structures are shown in Figures 5b, 5c and 5d, respectively.

TEM micrographs of LaS-CrS_2, CeS-CrS_2, GdS-CrS_2 and TbS-CrS_2 nanotubular structures synthesized by the above procedure are shown in Figure 6. Diffraction patterns produced from tubes of the $(LnS)_{1+y}TS_2$ MLC where (Ln=rare earths; T=Cr, V) are somewhat analogous to their PbS-NbS_2 counterparts.[16] However, CrS_2 and VS_2 exhibit octahedral (trigonal antiprismatic) coordination to S, which results in monoclinic or triclinic symmetry of both the TS_2 and the MS subsystem (with some exceptions).

Growth Mechanism of $(LnS)_{1+y}TS_2$ Nanotubes with (T=V, Cr). The growth mechanisms of lanthanide-based MLC nanotubes

dx.doi.org/10.1021/jz5016845 | J. Phys. Chem. Lett. 2014, 5, 3724−3736

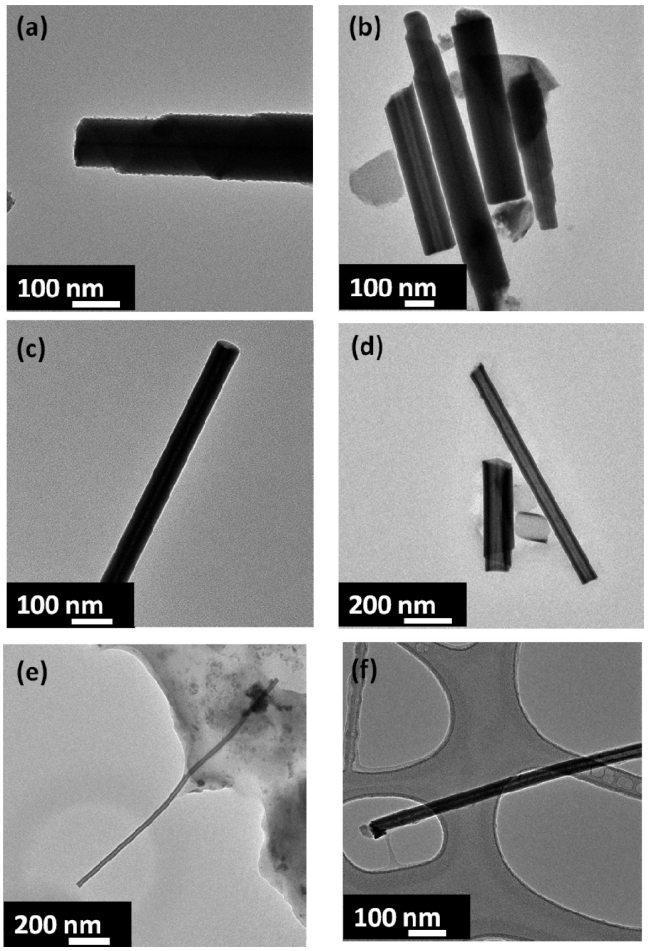

Figure 6. TEM images of nanoscrolls and nanotubes of (a) and (b) LaS-CrS_2, (c) and (d) CeS-CrS_2 (e) GdS-CrS_2 and (f) TbS-CrS_2.

synthesized by high temperature sulfurization of oxides or hydroxide mixtures are radically different from those of nanotubes obtained from chemical vapor transport discussed above. In the present case, treatment of preprepared ternary oxides with H_2S converts them to sulfides by a slow diffusion-controlled process. The difference between the oxide and sulfide densities (ca. 6.77 g cm^{-3} for $LaCrO_3$; 4.66 g cm^{-3} for $(LaS)_{1.2}CrS_2$) results in a significant volumetric change. At higher temperatures, the thermal expansion coefficients of the sulfides are generally higher than those of the oxides, which results in a further increase in strain upon conversion of the oxide to the respective sulfide. Sulfide nanowhiskers and nanosheets grow from the surface to minimize the stress generated across the interfaces, which are further scrolled by the misfit between the two sublattices. This mechanism is described schematically in Figure 7.

Figure 8 shows the *c*-axis periodicity of tubular structures synthesized from different MX-TS_2 MLC as a function of ion size. Several trends are apparent. For LnS-CrS_2 MLC with (Ln = Tb, Gd, Ce, La), the interplanar spacing increases with increasing M^{3+} ion size. For a particular LnS structure (LaS in this case), the *c*-axis periodicity is nearly independent of the choice of TX_2 and the spacings of LaS-CrS_2, LaS-VS_2 and LaS-TaS_2 are similar. However, the *c*-axis periodicities of the SnS-TaS_2 and PbS-TaS_2 structures are considerably larger when compared to nanotubes of the lanthanides, notwithstanding the smaller ionic size of the Sn atoms. This fact can be attributed to the smaller interaction

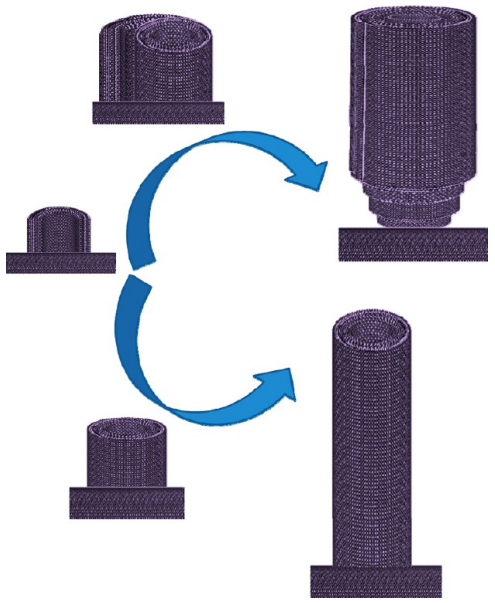

Figure 7. Schematic representation of nanotube and nanoscroll growth for a LnS-TS_2 MLC.

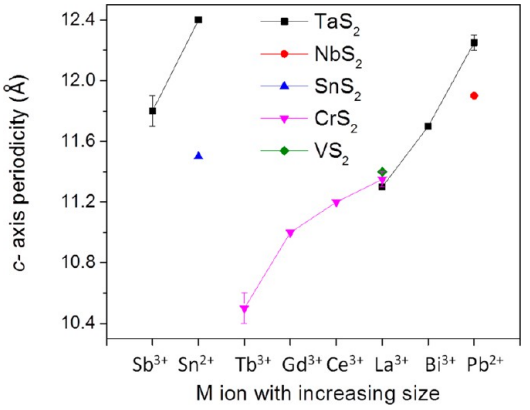

Figure 8. *c*-axis periodicity values of tubular structures from different MX-TX_2 MLC with O-T stacking order. The *x*-axis of the graph represents different MX compounds with increasing ionic radius of the M atoms.

(and smaller degree of charge transfer) between SnS or PbS with the TaS_2 layers, when compared to that with the LnS layers. This observation is not surprising in view of the fact that the VS_2 and CrS_2 structures do not exist in layered form in the bulk phase. It therefore appears that the donation of an electron from the LnS slab is essential for the formation of a 2D layered structure of CrS_2 (VS_2). Since the Ln ions are trivalent, significant charge transfer becomes possible and results in a strong interaction and smaller interplanar periodicity values along the *c*-axis. Bearing this in mind, the origin of the similarity between the periodicity values of LaS-TaS_2 and those of LaS-VS_2 and LaS-CrS_2 is unclear. In contrast to VS_2 and CrS_2, in which V and Cr prefer trivalent states, Ta adopts an oxidation state of +5. Therefore, TaS_2 exists as a bulk phase and does not require electron donation from the MS part. Furthermore, the additional 5d electron of Ta (since 4 participate in bonds with S atoms) is delocalized into the conduction band[26] and may be responsible for superconductivity at low temperature.[27]

The interlayer spacings of the SbS-TaS_2 and the BiS-TaS_2 structures are intermediate between those of the lanthanide-

dx.doi.org/10.1021/jz5016845 | J. Phys. Chem. Lett. 2014, 5, 3724−3736

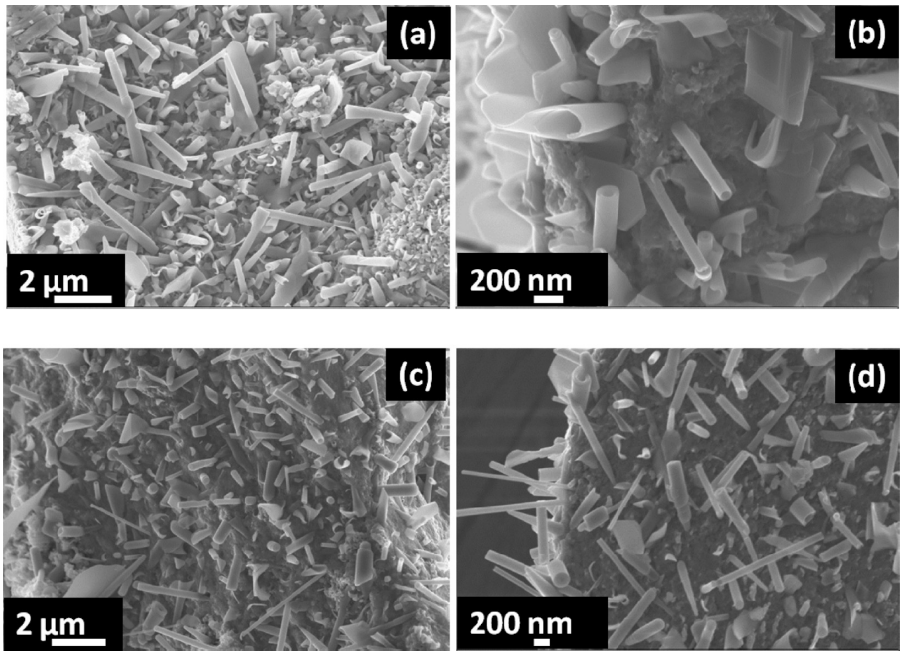

Figure 9. (a) low and (b) high magnification SEM images of 20 at% Sr substituted LaS-CrS_2 nanoscrolls and nanotubes. (c) low and (d) high magnification SEM images of 20 at% Ce substituted LaS-CrS_2 nanoscrolls and nanotubes.

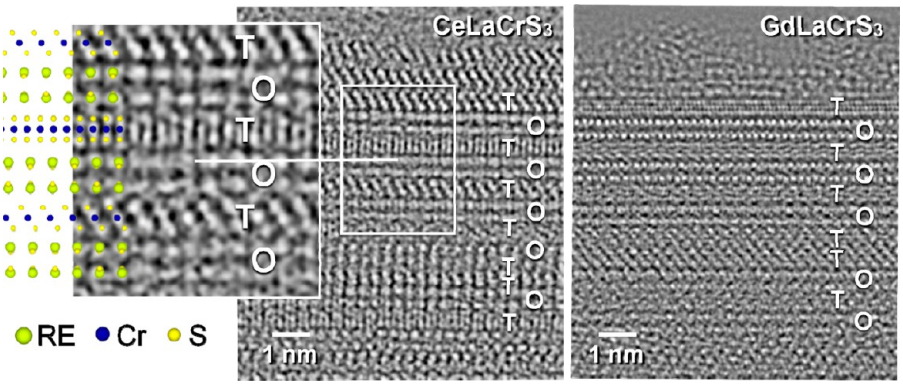

Figure 10. High-resolution TEM images of quaternary $CeLaCrS_3$ and $GdLaCrS_3$ nanotubes. The images show phases of exit-plane wave functions reconstructed from focal series data. A high density of the electrostatic atomic potential appears bright in thinner areas at the surfaces of the nanotubes.

based MLC and MS-TaS_2 with (M=Sn, Pb). Similarly to the lanthanides, Sb and Bi prefer trivalent states, in contrast to divalent Sn and Pb. Only two electrons from the Sb or Bi atoms are expected to participate in chemical bonds with S in the SbS or BiS lattice. Therefore, it is possible that the extra charge is partially transferred to the TaS_2 layer, as well as being accommodated in the Sb−Sb bonds at the antiphase boundaries as discussed above. However, the amount of charge transferred to TaS_2, if any, is expected to be small when compared to the charge transferred from the lanthanide sulfides to CrS_2 and VS_2. The higher values of interlayer spacing (*c*-axis) of PbS-TaS_2 relative to isostructural PbS-NbS_2 cannot be attributed to the slightly larger size of the Ta atoms, since the radii of the Nb and Ta atoms are equal. Also, a comparison between SnS-SnS_2 and SnS-TaS_2 is not straightforward. The ionic radii of Sn^{4+} and Ta^{4+} are almost the same. The differences in periodic interlayer spacing may be attributed to the formation of slightly different distorted structures as a result of a mutual structural modulation in the SnS-TaS_2 case, which is believed to be absent in SnS-SnS_2.[13]

Quaternary MLC Nanotubes. Quaternary nanotubular structures were obtained by substituting different di- and tri- valent ions (Sr^{2+}, Ce^{3+}, Eu^{2+}, Gd^{3+}) in the parent nanotubes. SEM images of Sr-substituted and Ce-substituted $LaCrS_3$ are shown in Figure 9. Vacancies were proposed to exist in the lanthanide subunits of the MLC. These vacancies maintain charge balance between the Ln^{3+}, Cr^{3+} and S^{2-} ions in the lattice.[28] Divalent Sr^{2+} can be substituted in bulk $(LaS)_{1.2}CrS_2$ up to 20 at%. Exceeding this limit results in inhibition of the formation of the misfit structure.[29] This limit was attributed to La^{3+} vacancies in the LaS sublattice, which can reach up to 6%, i.e., $(La_{0.94}[V_{0.06}]S)_{1.2}CrS_2$ $\{(LaS)[La_{2/3}[V]_{1/3}S]_{0.2}CrS_2\}$. This formula predicts exact charge balance between the La^{3+}, Cr^{3+} and S^{2-} ions, with complete charge transfer from the La to the Cr atoms. A substitution arrangement implies that three Sr^{2+} ions replace two La^{3+} ions and that one vacancy is filled. Therefore, by adding up to 20% of the binary Sr^{2+} or Eu^{2+} ions into the LaS lattice, the La vacancies become fully occupied without violating the criterion for charge balance in the $LaCrS_3$ lattice. Similarly, substitution of up to 20 at % of the divalent ions, such as Sr^{2+} and Eu^{2+} (Eu forms a divalent ion under reducing conditions), in the $LaCrS_3$ nanotubes could be realized. Higher concentrations of the divalent metal ions

dx.doi.org/10.1021/jz5016845 | J. Phys. Chem. Lett. 2014, 5, 3724−3736

inhibited the formation of MLC and led to the formation of nanowhiskers instead of nanotubes/nanoscrolls.[16]

Figure 10 shows high-resolution TEM images of the sequence of triatomic layers in the outer shells of quaternary Ce^{3+} and Gd^{3+} substituted $LaCrS_3$. Phase images reconstructed from focal series show atomic strings as bright dots. Hexagonal triple-atom layers and rock-salt layers are visible directly. Interestingly, Ce^{3+} and Gd^{3+} substitution in $LaCrS_3$ nanotubes resulted in superstructure polytypism. In the quaternary compounds, one sporadically finds O-T-O-T-T-O-T-O-T-T··· superstructures that contain double layers of CrS_2, besides the commonly observed O-T-O-T··· superstructure in the ternary MLC. This situation is most readily apparent for 20 at% Gd^{3+} substitution (Figure 10 and ref.[16]). This observation leads to two views: (i) the amount of charge transfer needed to stabilize CrS_2 layers is less than one electron per formula unit (at least in nanotubular form) or (ii) each formula unit of GdS or CeS gives more than one electron to CrS_2 which is less likely. Trivalent ion substitution is similar to that of divalent ion substitution except that one La^{3+} is replaced by one Gd^{3+}. Apart from that 6 at% of La vacancies can also be filled by Gd^{3+}, thus having extra charge on the lanthanide sublayer compared to unsubstituted one. It is believed that this extra charge in lanthanide sublayer is facilitating the formation of the O-T-O-T-T··· super structure in quaternary MLC. Some disorder in the superstructure, which may possibly be attributed to the substitution of La by Ce(Gd), is also apparent in the present case. Further research is needed to clarify this point.

The ratio of nanotubes vs nanoscrolls in the MLC nanotubes is mainly observed to be dependent on the symmetry of the structure.

Nanotubes vs Nanoscrolls. The ratio of nanotubes vs nanoscrolls in the MLC nanotubes is mainly observed to be dependent on the symmetry of the structure and less significantly on the reaction conditions, such as the rate of heating. The above observation is not surprising in the sense that the symmetry of the unit cell dictates the ability to seam facets. If the lattice is more complex, then additional boundary conditions need to be imposed to form a stable and seamless closed nanostructure.[30] Therefore, MLC with relatively high symmetry crystals, such as $GdCrS_3$ and $TbCrS_3$ with orthorhombic structures, can produce closed structures (nanotubes) more easily. In contrast, nanoscrolls are abundant in low symmetry MLC crystals, such as $LaCrS_3$ with a triclinic structure. Since the nanotubes are produced by a kinetically controlled reaction, it is not unexpected to find that the rate of heating also has an influence on the product yield and the nanotube vs nanoscroll ratio. Rapid heating was found to favor nanotube production. The aspect ratio of the MLC nanotubes is in general higher than that of nanoscrolls in the product synthesized by the high temperature conversion of oxide to sulfide. In a given material, the average diameters of the nanotubes are smaller than that of the nanoscrolls and they are longer. Since the mass transport is the same for the nanotubes and the nanoscrolls (the chemical composition is the same), the total mass of the product is the same, irrespective of the product.

Interaction between the Layers. Misfit compounds are considered to be stabilized, at least partially, by charge transfer between adjacent layers. The degree of charge transfer depends on the work functions of the two subunits. CrS_2 and VS_2 are unstable in hexagonal (layered) form.[5] Charge transfer from the MX layer then introduces stability to the hexagonal layered structure of the TS_2 subsystem. On the other hand, since SnS_2, NbS_2, *etc.* possess stable layered structures, charge transfer between the two constituent sublattices is not required to form stable misfit structures. Measurements of the amount of charge transfer between the two subunits exist but are controversial.[5,15,20,23] The degree of charge transfer also affects the stacking order in misfit compounds. A one-to-one stacking order (O-T-O-T···), i.e., an MS layer adjacent to a TS_2 layer, is required to create a CrS_2 (VS_2)-based MLC. In contrast, SnS_2 based misfit compounds, in which charge transfer effects are weaker, exhibit more than one type of periodicity, including O-T-O-T···, O-T-T-O-T-T···, and O-T-O-T-T-O-T-O-T-T···. Also the possibility of weak covalent bonding between M and X atoms in TX_2 has been mentioned in the literature,[31,32] however, further experimental studies are needed to verify this hypothesis. Theoretical studies of misfit nanotubes have been quite scarce. However, recently Lorenz et al. carried out DFT calculations for SnS-SnS_2 nanotubes.[33] They found that the interaction between the SnS and SnS_2 layers goes beyond a van-der-Waals interaction. Surprisingly, in contrast to common wisdom, which suggests charge transfer from MX to TX_2,[34,35] they observed that a small but discernible charge is transferred from the SnS_2 to the SnS layer. This somewhat counterintuitive observation was attributed to the interaction between the SnS and the SnS_2 monolayers.[33]

Folding Mechanism. The strain that results from the lattice mismatch between the in-plane lattice parameters of the individual layers is believed to be the main driving force for curling. The tubule axis is expected to be perpendicular to the direction along which the lattice parameters differ by the largest amount (usually the *a*-axis). However, experimental observations show that this is not always the case.[15,16] The misfit is decreased by bending the layers and consequently the strain energy is reduced. Bending is expected to be spontaneous for asymmetric layers that consist of an MX slab on one side and a TX_2 layer on the other side.[9] The thinner the wall, the greater is the deformation in response to the bending moment resulting from the lattice mismatch, i.e., the smaller is the nanotube radius that can be formed. A sufficiently large driving force for spontaneous bending is observed only in very thin and asymmetric layers. Once a tubule with the first few walls has formed, it can serve as a nucleus (template) for further thickening of the nanotube's wall. The TX_2 layers have a pseudohexagonal unit cell with 6-fold symmetry of the ⟨10.0⟩ and ⟨11.0⟩ directions (⟨020⟩ and ⟨200⟩ in the ortho-pseudohexagonal system, respectively). Therefore, the [020] direction of the MX layer can be superimposed onto the [020] direction of the TX_2 layer in three crystallographically equivalent ways. Layers of TX_2 and MX with different folding vectors can then occur within the same tubule. However, the orientations of the layers that have different folding vectors relative to the tubule axis are different. In several cases, SAED studies of tubular crystals show ring-like patterns of spots for both the MX and the TX_2 layers. These ring-like patterns are very common in tubular structures of SbS-TaS_2 MLC and also for conical tubules (nanoscrolls) in PbS-NbS_2, PbS-TaS_2 and SnS-TaS_2 MLC. Cylindrical tubules that exhibit ring-like patterns in PbS-NbS_2 and PbS-TaS_2 MLC have also been encountered, albeit rarely. These ring-like patterns suggest the presence of a turbostratic (rotational) misorientation of the layers about the common *c*-axis. Turbostratic disorder is commonly observed in some MLC nanotubes that show some

dx.doi.org/10.1021/jz5016845 | J. Phys. Chem. Lett. 2014, 5, 3724−3736

extent ferecrystal behavior and are known to have very low thermal conductivity.[36]

The strain that results from the lattice mismatch between the in-plane lattice parameters of the individual layers is believed to be the main driving force for curling.

Misfit nanotubes sometimes show goffering behavior (wave-like fringes and some periodic shades perpendicular to the tube axis).[13] This phenomenon may be attributed to yet another stress relaxation mechanism. This behavior is observed frequently in O-T type nanotubes, where the misfit strain per unit volume is higher than in O-T-T or O-T-O-T-T nanotubes.[13] SAED patterns of these tubes differ from those acquired from normal nanotubes. A semiquantitative explanation for the observed diffraction patterns of goffered nanotubes was offered by Figovsky et al.[37]

Physical Properties. The perovskite (ABO_3) structures of ternary oxides can be regarded as being made up of alternating AO and BO_2 layers.[38] Compounds with these structures are known to have many interesting properties, including superconductivity, ferroelectricity and magnetoresistance.[39−44] Stackings of MX and TX_2 layers in MLC can be thought of as analogous to AO and BO_2 layers in perovskite sructures and may therefore exhibit novel structure-related properties. MLC are predicted to show superior thermoelectric behavior due to their unique structures, in which electron transport takes places along the *a*-*b* planes of one subsystem, while the other sublattice serves as a phonon barrier.[45,46] Furthermore, superior thermoelectric properties are favored in reduced dimensions.[47] The intrinsic structural properties of MLC, along with their one-dimensional nanostructure, could further improve their thermoelectric properties. Testing the thermoelectric properties of individual nanotubes should therefore be an interesting and highly warranted endeavor. Superconductivity has also been observed in MLC.[27,48,49] However, superconductivity in purely one-dimensional systems has been debated.[50] Studying such phenomena in misfit nanotubes, which are quasi-one-dimensional systems with (quite) perfectly crystalline structures, is of great fundamental interest.

Selenides and tellurides are known to show superior thermoelectric and superconducting properties. The synthesis of misfit nanotubes from these compounds and studies of their properties is a pressing future challenge. Also misfit layered oxides are interesting candidates to study.

Optical Properties. Lanthanides play a major role in light-emitting devices, especially in (Er- and Tb-based) commercial lasers for optical communication and in (Eu- and Tb-based) medical devices.[51−53] The lasing action in lanthanides involves deep 4f-shells, which are not significantly affected by their environment. Because 4f−4f absorptions are parity-forbidden, lanthanide-based compounds show very low molar absorption coefficients (less than 3 M^{-1} s^{-1}). The incorporation of lanthanide ions in semitransparent matrices is often used to achieve optically pumped emission. Lanthanide-based misfit compounds show low extinction coefficients in the visible and near IR. Composites made from these compounds and semitransparent matrices should therefore be explored.

Two-dimensional materials including graphene, graphene-like materials and transition metal dichalcogenides exhibited immense potential as electrocatalysts because of the possibility of tuning their properties on a molecular basis.[54−58] Alternatively, misfit layered compounds have also recently shown to be potential candidates as electrocatalysts.[59] The misfit layered oxide $Ca_3Co_4O_9$ was tested for hydrogen evolution and oxygen reduction and was found to be a promising candidate as an electrocatalyst.[59] These properties in principle should be enhanced in reduced dimensions.

Recent developments in the synthesis and structural characterization of nanotubes from misfit layered compounds have been described in this "Perspective". These nanostructures are new members in the broad field of inorganic nanotubes of 2D crystals. It is believed that they are of great interest, not only from the point of view of structural complexity, but because they may also reveal new physical properties that are related to their unique structures and low dimensionalities.

AUTHOR INFORMATION

Corresponding Author

*E-mail: Reshef.Tenne@weizmann.ac.il.

Author Contributions

[‖](L.S.P., G.R.) Equal contribution.

Notes

The authors declare no competing financial interest.

Biographies

Leela S. Panchakarla received his Ph.D. degree from the Jawaharlal Nehru Centre for Advanced Scientific Research, Bangalore under the supervision of Prof. C. N. R. Rao. He worked as a postdoctoral research associate in the group of Prof. M. Samy El-Shall in Virginia Commonwealth University, USA. Presently he is a postdoctoral fellow in Prof. Reshef Tenne's group at the Weizmann Institute of Science. He is presently working on misfit layered nanotubes.

Gal Radovsky received his B.Sc. (2007) and M.Sc. (2009) degrees in Materials Engineering from the Ben-Gurion University (Israel). He completed his Ph.D. (2014) degree studying misfit compound nanotubes at the department of Materials and Interfaces of the Weizmann Institute of Science (Israel) under the supervision of Prof. Reshef Tenne. He currently holds a postdoctoral position in the same group.

Lothar Houben received his Ph.D. degree in Physics in 1998 from the Heinrich-Heine-Universität Düsseldorf. He is a research staff member in the Ernst Ruska-Centre for Microscopy and Spectroscopy with Electrons in Forschungszentrum Jülich.

Ronit Popovitz-Biro received her Ph.D. (1980) degree in chemistry from the Weizmann Institute of Science, Rehovot, Israel. From 1982−1984, she was a postdoctoral research fellow in the Chemistry Department of the University of California at San Diego (UCSD). From 1986−1997, she was an associate staff scientist in the Department of Materials and Interfaces, Weizmann Institute of Science. Since 1998 she has been a senior staff scientist in the electron-microscopy unit, in the Department of Chemical Research Support of the Weizmann Institute of Science.

Rafal Dunin-Borkowski is the Director of the Ernst Ruska-Centre for Microscopy and Spectroscopy with Electrons in Forschungszentrum Jülich. Between 2007 and 2010, he led the establishment of the Center for Electron Nanoscopy in the Technical University of Denmark. In 2009 he received the Ernst Ruska Prize of the German Society for Electron Microscopy. In 2012 he received an Advanced Grant from the European Research Council.

Reshef Tenne earned his Ph.D. in 1976 in physical chemistry in the Hebrew University. He joined the Weizmann Institute in 1979 and was promoted to professor in 1995. His interests are focused on the synthesis and study of nanotubes and fullerene-like nanoparticles of layered compounds, like WS_2, which he discovered in 1992. He is the recipient of, among others, the Materials Research Society (MRS) Medal, the Israel Chemical Society Prize (2008), and the European Research Council (ERC) Advanced Research Grant (2008). He is a member of the Israel Academy of Sciences and Academia Europaea and Fellow of the Royal Society of Chemistry. Homepage: http://www.weizmann.ac.il/materials/tenne/.

■ ACKNOWLEDGMENTS

This study was supported by a grant from the Israel Science Foundation; EU ITN MoWSeS 317451 grant. We acknowledge the support of the Harold Perlman; the Irving and Azelle Waltcher Foundations in honor of Prof. M. Levy; the G.M.J. Schmidt Minerva Center for Supramolecular Chemistry and the Irving and Cherna Moskowitz Center for Nano and Bio-Nano Imaging. R.T. holds the Drake Family chair in Nanotechnology and is the director of the Helen and Martin Kimmel Center for Nanoscale Science. L.S.P. would like to thank the PBC Program of the Government of Israel for a postdoctoral fellowship. The research has received funding from the EU FP7 Programme under Grant Agreement 312483 - ESTEEM2 (Integrated Infrastructure Initiative−I3).

■ REFERENCES

(1) Iijima, S. Helical Microtubules of Graphitic Carbon. *Nature* **1991**, *354*, 56−58.
(2) Tenne, R.; Margulis, L.; Genut, M.; Hodes, G. Polyhedral and Cylindrical Structures of Tungsten Disulphide. *Nature* **1992**, *360*, 444−446.
(3) Tenne, R. Inorganic Nanotubes and Fullerene-Like Nanoparticles. *Nat. Nanotechnol.* **2006**, *1*, 103−111.
(4) Rao, C. N. R.; Govindaraj, A. *Nanotubes and Nanowires*; RSC Publishing: Cambridge, UK, 2005.
(5) Wiegers, G. A. Misfit Layered Compounds: Structures and Physical Properties. *Prog. Solid St. Chem.* **1996**, *24*, 1−139.
(6) Makovicky, E.; Hyde, B. G. Non-Commensurate (Misfit) Layer Structures. In *Inorganic Chemistry*; Structure and Bonding Series; Springer Verlag: Heidelberg, 1981; Vol. *46*, p 101.
(7) Wiegers, G. A.; Meerschaut, A. Incommensurate Sandwiched Layered Compounds. In *Materials Science Forum*; Meerschaut, A., Ed.; Trans Tech Publications: Pfaffikon, Switzerland, 1992; Vols. *100 & 102*, pp 101.
(8) Seifert, G.; Kohller, T.; Tenne, R. Stability of Metal Chalcogenide Nanotubes. *J. Phys. Chem. B* **2002**, *106*, 2497−2501.
(9) Bernaerts, D.; Amelinckx, S.; Van Tendeloo, G.; Van Landuyt, J. Microstructure and Formation Mechanism of Cylindrical and Conical Scrolls of the Misfit Layer Compounds $PbNb_nS_{2n+1}$. *J. Cryst. Growth* **1997**, *172*, 433−439.
(10) Hong, S. Y.; Popovitz-Biro, R.; Prior, Y.; Tenne, R. Synthesis of SnS_2/SnS Fullerene-Like Nanoparticles: A Superlattice with Polyhedral Shape. *J. Am. Chem. Soc.* **2003**, *125*, 10470−10474.
(11) Gomez-Herrero, A.; Landa-Canovas, A. R.; Otero-Diaz, L. C. Electron Microscopy Study of Tubular Crystals $(BiS)_{1+d}(NbS_2)_n$. *Micron* **2000**, *31*, 587−595.
(12) Radovsky, G.; Popovitz-Biro, R.; Staiger, M.; Gartsman, K.; Thomsen, C.; Lorenz, T.; Seifert, G.; Tenne, R. Synthesis of Copious Amounts of SnS_2 and SnS_2/SnS Nanotubes with Ordered Superstructures. *Angew. Chem., Int. Ed.* **2011**, *50*, 12316−12320.
(13) Radovsky, G.; Popovitz-Biro, R.; Tenne, R. Study of Tubular Structures of the Misfit Layered Compound SnS_2/SnS. *Chem. Mater.* **2012**, *24*, 3004−3015.
(14) Radovsky, G.; Popovitz-Biro, R.; Stroppa, D. G.; Houben, L.; Tenne, R. Nanotubes from Chalcogenide Misfit Compounds: Sn−S and Nb−Pb−S. *Acc. Chem. Res.* **2014**, *47*, 406−416.
(15) Radovsky, G.; Popovitz-Biro, R.; Tenne, R. Nanotubes from the Misfit Layered Compounds MS−TaS_2, where M = Pb, Sn, Sb, or Bi: Synthesis and Study of their Structure. *Chem. Mater.* **2014**, *26*, 3757−3770.
(16) Panchakarla, L. S.; Popovitz-Biro, R.; Houben, L.; Dunin-Borkowski, R. E.; Tenne, R. Lanthanide-Based Functional Misfit-Layered Nanotubes. *Angew. Chem., Int. Ed.* **2014**, *53*, 6920−6924.
(17) Cario, L.; Corraze, B.; Meerschaut, A.; Moelo, Y.; Chauvet, O. Electronic Properties of the $(LaS)_{1.18}VS_2$ Incommensurate Misfit Compound. *Synt. Met.* **1999**, *103*, 2640−2643.
(18) Del Buccia, P. S.; Jumas, J. C.; Maurin, M. Contribution à L'étude de Composés Sulfurés D'étain(II): Affinement De La Structure De SnS. *Acta Crystallogr. Sect. B* **1981**, *37*, 1903−1905.
(19) Mitchell, R. S.; Fujiki, Y.; Ishizawa, Y. Structural Polytypism of SnS_2. *Nature* **1974**, *247*, 537−538.
(20) Espinos, J. P.; Gonzalez-Elipe, A. R.; Jumas, J. C.; Olivier-Fourcade, J.; Morales, J.; Tirado, J. L.; Lavela, P. Sb Mossbauer and X-ray Photoelectron Spectroscopy Studies of the Electronic Structure of Some Antimony Misfit Layer Compounds. *Chem. Mater.* **1997**, *9*, 1393−1398.
(21) Ren, Y.; Meetsma, A.; Petricek, V.; Van Smaalen, S.; Wiegers, G. A. (3 + 2)-Dimensional Superspace Approach to the Structure of the Incommensurate Intergrowth Compound: $(SbS)_{1.15}TiS_2$. *Acta Crystallogr. B* **1995**, *51*, 275−287.
(22) Kars, M.; Fredrickson, D. C.; Gomez-Herrero, A.; Lidin, S.; Rebbah, A.; Otero-Diaz, L. C. Structural Study by X-ray Diffraction and Transmission Electron Microscopy of the Misfit Compound $(SbS_{1-x}Se_x)_{1.16}(Nb_{1.036}S_2)_2$. *Mater. Res. Bull.* **2010**, *45*, 982−988.
(23) Ren, Y.; Haas, C.; Wiegers, G. A. Photoelectron Spectroscopy Study of the Electronic Structure of the Incommensurate Intergrowth Compounds $(SbS)_{1.15}(TiS_2)_n$ with n = 1,2. *J. Phys.: Condens. Matter* **1995**, *7*, 5949−5958.
(24) Meetsma, A.; Wiegers, G. A.; Haange, R. J.; De Boer, J. L. Structure of 2H-TaS_2. *Acta Cryst.C* **1990**, *46*, 1598−1599.
(25) Murugesan, T.; Ramesh, S.; Gopalakrishnan, J.; Rao, C. N. R. Rare Earth Transition Metal Sulfides, $LnMS_3$. *J. Solid State Chem.* **1981**, *38*, 165−172.
(26) Di Salvo, F. J. Charge Density Waves in Layered Compounds. *Surf. Sci.* **1976**, *58*, 297−311.
(27) Schmidt, L. Superconductivity in $PbNbS_3$ and $PbTaS_3$. *Phys. Lett. A* **1970**, *31*, 551−552.
(28) Rouxel, J.; Moelo, Y.; Lafond, A.; Disalvo, F. J.; Meerschaut, A.; Roesky, R. Role of Vacancies in Misfit Layered Compounds: The Case of the Gadolinium Chromium Sulfide Compound. *Inorg. Chem.* **1994**, *33*, 3358−3363.
(29) Cario, L.; Johrendt, D.; Lafond, A.; Felser, C.; Meerschaut, A.; Rouxel, J. Stability and Charge Transfer in the Misfit Compound $(LaS)(SrS)_{0.2}CrS_2$: Ab Initio Band-Structure Calculations. *Phys. Rev. B* **1997**, *55*, 9409−9414.
(30) Levi, R.; Bar-Sadan, M.; Albu-Yaron, A.; Popovitz-Biro, R.; Houben, L.; Shahar, C.; Enyashin, A.; Seifert, G.; Prior, Y.; Tenne, R. Hollow V_2O_5 Nanoparticles (Fullerene-Like Analogues) Prepared by Pulsed Laser Ablation. *J. Am. Chem. Soc.* **2010**, *132*, 11214−11222.
(31) Ettema, A. R. H. F.; Haas, C. Electronic Structure of the Misfit-Layer Compound $(SnS)_{1.17}NbS_2$ Deduced from Band-Structure Calculations and Photoelectron Spectra. *J. Phys.: Condens. Matter* **1993**, *5*, 3817−3826.
(32) Fang, C. M.; Ettema, A. R. H. F.; Haas, C.; Wiegers, G. A. Electronic Structure of the Misfit-Layer Compound $(SnS)_{1.17}NbS_2$ Deduced from Band-Structure Calculations and Photoelectron Spectra. *Phys. Rev. B* **1995**, *52*, 2336−2347.
(33) Lorenz, T.; Joswig, J.-O.; Seifert, G. Combined SnS@SnS_2 Double Layers: Charge Transfer and Electronic Structure. *Semicond. Sci. Technol.* **2014**, *29*, 064006.
(34) Wiegers, G. A. Charge Transfer between Layers in Misfit Layer Compounds. *J. Alloys Comp.* **1995**, *219*, 152−156.

(35) Meerschaut, A.; Moelo, Y.; Cario, L.; Lafond, A.; Deudon, C. Charge Transfer in Misfit Layer Chalcogenides, $[(MX)_n]_{1+x}(TX_2)_m$: A Key for Understanding their Stability and Properties. *Mol. Cryst. Liq. Cryst. Bull.* **2000**, *341*, 1−8.
(36) Beekman, M.; Heideman, C. L.; Johnson, D. C. Ferecrystals: Non-Epitaxial Layered Intergrowths. *Semicond. Sci. Technol.* **2014**, *29*, 064012.
(37) Figovsky, O.; Pashin, D.; Khalitov, Z.; Valeeva, D.; Chkanov, A. The Pecularities of Structure and Diffraction by Misfit Mixed-Layer Nanotubes. *Int. Lett. Chem., Phys. Astron.* **2012**, *2*, 7−14.
(38) Galasso, F. S. *Structure, Properties, and Preparation of Perovskite-Type Compounds*; Pergamon Press: Oxford, U.K., 1969.
(39) Bednorz, J. G.; Muller, K. A. Possible High T_c Superconductivity in the Ba−La−Cu−O System. *Z. Phys. B* **1986**, *64*, 189.
(40) von Helmolt, R.; Wecker, J.; Holzapfel, B.; Schultz, L.; Samwer, K. Giant Negative Magnetoresistance in Perovskite like $La_{2/3}Ba_{1/3}MnO_x$ Ferromagnetic Films. *Phys. Rev. Lett.* **1993**, *71*, 2331−2333.
(41) McCormack, M.; Jin, S.; Tiefel, T. H.; Fleming, R. M.; Phillips, J. M.; Ramesh, R. Very Large Magnetoresistance in Perovskite-like La−Ca−Mn−O Thin Films. *Appl. Phys. Lett.* **1994**, *64*, 3045−3047.
(42) Jin, S.; Tiefel, T. H.; McCormack, M.; Fastnacht, R. A.; Ramesh, R.; Chen, L. H. Thousand Fold Change in Resistivity in Magnetoresistive La−Ca−Mn−O Films. *Science* **1994**, *264*, 413−415.
(43) Urushibara, A.; Moritomo, Y.; Arima, T.; Asamitsu, A.; Kido, G.; Tokura, Y. Insulator− Metal Transition and Giant Magnetoresistance in $La_{1-x}Sr_xMnO_3$. *Phys. Rev. B* **1995**, *51*, 14103−14109.
(44) Mahendiran, R.; Raychaudhuri, A. K.; Chainani, A.; Sarma, D. D.; Roy, S. B. Large Magnetoresistance in $La_{1-x}Sr_xMnO_3$ and its Dependence on Magnetization. *Appl. Phys. Lett.* **1995**, *66*, 233−235.
(45) Slack, G. A. In *CRC Handbook of Thermoelectric*; Rowe, D. M., Ed.; CRC Press: Boca Raton FL, 1995; pp 407−440.
(46) Putri, E.; Wan, C.; Wang, Y.; Norimatsu, W.; Kusunoki, M.; Koumoto, K. Effects Of Alkaline Earth Doping on the Thermoelectric Properties of Misfit Layer Sulfides. *Scripta Mater.* **2012**, *66*, 895−898.
(47) Hicks, L. D.; Dresselhaus, M. S. Thermoelectric Figure of Merit of a One-Dimensional Conductor. *Phys. Rev. B* **1993**, *47*, 16631−16634.
(48) Reefman, D.; Baak, J.; Brom, H. B.; Wiegers, G. A. Superconductivity in Misfit Layer Compounds $(MS)_nTS_2$. *Solid State Commun.* **1990**, *75*, 47−51.
(49) Schmidt, L.; McCarthy, S. L.; Maita, J. P. Superconducting Behavior of the System $Pb(Nb_{1-x}Ta_x)S_3$. *Solid State Commun.* **1970**, *8*, 1513−1515.
(50) Kociak, M.; Kasumov, A. Y.; Guéron, S.; Reulet, B.; Khodos, I. I.; Gorbatov, Y. B.; Volkov, V. T.; Vaccarini, L.; Bouchiat, H. Superconductivity in Ropes of Single-Walled Carbon Nanotubes. *Phys. Rev. Lett.* **2001**, *86*, 2416−2419.
(51) Bunzli, J.-C. G.; Piguet, C. Taking Advantage of Luminescent Lanthanide Ions. *Chem. Soc. Rev.* **2005**, *34*, 1048−1077.
(52) Binnemans, K. Lanthanide-Based Luminescent Hybrid Materials. *Chem. Rev.* **2009**, *109*, 4283−4374.
(53) Bünzli, J.-C. G. Lanthanide Luminescence for Biomedical Analyses and Imaging. *Chem. Rev.* **2010**, *110*, 2729−2755.
(54) Chen, D.; Tang, L.; Li, J. Graphene-Based Materials in Electrochemistry. *Chem. Soc. Rev.* **2010**, *39*, 3157−3180.
(55) Brownson, D. A. C.; Kampouris, D. K.; Banks, C. E. Graphene Electrochemistry: Fundamental Concepts through to Prominent Applications. *Chem. Soc. Rev.* **2012**, *41*, 6944−6976.
(56) Choi, C.; Feng, J.; Li, Y.; Wu, J.; Zak, A.; Tenne, R.; Dai, H. WS_2 Nanoflakes from Nanotubes for Electrocatalysis. *Nano Res.* **2013**, *6*, 921−928.
(57) Cheng, L.; Huang, W.; Gong, Q.; Liu, C.; Liu, Z.; Li, Y.; Dai, H. Ultrathin WS_2 Nanoflakes as a High-Performance Electrocatalyst for the Hydrogen Evolution Reaction. *Angew. Chem., Int. Ed.* **2014**, *53*, 7860−7863.
(58) Moses, K.; Kiran, V.; Sampath, S.; Rao, C. N. R. Few-Layer Borocarbonitride Nanosheets: Platinum-Free Catalyst for the Oxygen Reduction Reaction. *Chem.—Asian J.* **2014**, *9*, 838−843.
(59) Lim, C. S.; Chua, C. K.; Sofer, Z.; Jankovský, O.; Pumera, M. Alternating Misfit Layered Transition/Alkaline Earth Metal Chalcogenide $Ca_3Co_4O_9$ as a New Class of Chalcogenide Materials for Hydrogen Evolution. *Chem. Mater.* **2014**, *26*, 4130−4136.